Device-free Counting via Wideband Signals

Stefania Bartoletti, *Member, IEEE*, Andrea Conti, *Senior Member, IEEE*, and Moe Z. Win, *Fellow, IEEE*

***Abstract*—Counting people and things (targets) in a monitored area, also known as crowd-counting, enables several applications in diverse scenarios including smart building, intelligent transportation, and public safety. In many scenarios, device-free systems relying on the signal backscattering from targets are preferred to device-based systems relying on the communication with the targets via dedicated or personal devices. However, the use of conventional radar techniques (e.g., for multi-target detection) requires to associate a different set of measured data with each detected target. Data association is a redundant operation for counting and results in high complexity even with few targets. The need of lower dimensionality and complexity calls for signal features to associate the measured signals directly with the number of targets. This paper proposes a mathematical framework for the design of device-free counting systems. First, a maximum a posteriori algorithm is developed for counting via wideband signal backscattering by relying on model order selection. Then, a method that relies on low-level features is proposed to lower the computational complexity. The proposed method is verified via sample-level simulations in realistic operating conditions and compared to current solutions.**

***Index Terms*—Counting, sensor radar, device-free, multi-target detection, multi-hypothesis testing, wideband signals.**

I. Introduction

DEVICE-FREE COUNTING refers to the estimation of the number of people and things (hereafter referred to as targets) in a monitored area without relying on any dedicated or personal device. Counting targets is crucial for several crowdsensing and behaviour analysis applications, in diverse scenarios including smart building, intelligent transportation, and public safety [1]–[3].

Current counting systems are classified as image-based and radio-based. In both cases, data collected from multiple sensors are processed to infer the number of targets by relying on statistical models or training sequences. In image-based systems, the counting is performed by processing the foreground image after removal of the background image [4]–[6]. For example, the number of foreground pixels is counted and the number of targets is then determined by considering the target size within the image, which changes according to the geometry of the vision system. Image-based systems are resource-intensive, suffer from obstructed line-of-sight conditions and are sensitive to light and colors, and their use is often denied for privacy. Therefore, in many scenarios, radio-based systems replace or operate jointly with image-based systems.

Radio-based systems can be further classified as device-based and device-free. In device-based systems, the counting is either performed by counting the number of targets equipped with dedicated devices, such as radio frequency identification (RFID) tags [7]–[9], or sniffed from personal devices, such as from Wi-Fi access points [10]–[15]. In the former case, the cost of providing each target with a dedicated device is unaffordable for many applications. In the latter case, the counting system needs access to the network of users, which is not always possible (e.g., safety applications) and also leads to major privacy issues, especially when the system exploits personal devices. Alternatively, device-free systems have been recently investigated. In such systems, target counting is performed by sensing the wireless environment to infer the number of targets from signal reflections and obstructions (e.g. by employing sensor radar networks) [16]–[20]. The two main advantages of device-free systems with respect to device-based systems are: (i) lower implementation costs and (ii) higher privacy preservation. In fact, they do not need to access any user network, and they do not require dedicated devices to be carried by targets.

Current algorithms for device-free counting rely on multi-target detection via radar networks [19]–[22]. In multi-target detection, a different set of measurements is associated with each detected target, for example, by estimating its position and trajectory, and the number of targets is then deduced. This method is also known as *individual-centric*. However, individual-centric methods have high complexity growing exponentially with the number of targets due to data association, which is unnecessary when the system is interested in only the number of targets and not their locations. For these reasons, there is a growing interest in designing *crowd-centric* methods for counting, i.e., methods that infer the number of targets directly from the measured data without estimating their locations [16]–[18].

Among device-free systems, sensor radars based on wideband and ultrawide-band (UWB) signals [23]–[25] are good candidates for counting because the wide bandwidth provides fine delay resolution, which mitigates multipath and allows the detection of multiple targets that are close in space [26]–[34]. In [16], a method is proposed to count targets moving in and out of a monitored area by using a UWB radar at the entrance of the area to estimate the time-of-arrival (TOA)

Manuscript received September 22, 2016; revised January 13, 2017; accepted January 26, 2017. Date of publication MONTH XX, YYYY; date of current version MONTH XX, YYYY. This research was supported, in part, by the European Union's Horizon 2020 research and innovation programme under the Marie Skłodowska-Curie Grant 703893, the Office of Naval Research under Grant N00014-16-1-2141, and the MIT Institute for Soldier Nanotechnologies.

S. Bartoletti is with ENDIF, University of Ferrara, Italy, and the Wireless Information and Network Sciences Laboratory, Massachusetts Institute of Technology, Cambridge, MA 02139, USA (e-mail: stefania.bartoletti@unife.it).

A. Conti is with ENDIF, University of Ferrara, Italy (e-mail: a.conti@ieee.org).

M. Z. Win is with the Laboratory for Information and Decision Systems (LIDS), Massachusetts Institute of Technology, Cambridge, MA 02139 USA (e-mail: moewin@mit.edu).

Digital Object Identifier XX.XXXX/JSAC.XXXX.XXXXXXX

of backscattered signals. This method requires the design of threshold-crossing techniques for the direction estimation based on TOA. In [17], a counting algorithm is proposed for UWB radar, based on the local maximum of the power profile of the received waveform. Iteratively, a local maximum is searched and, in case it exceeds a threshold, a set of samples (window) around the local maximum is deleted. The two aforementioned methods do not provide any algorithm to design the thresholds and window's length, which are crucial for the system performance [26]. In [18], the crowd-centric counting is addressed by using support vector regression (SVR) to learn the relation between the extracted features and the number of targets. Such features belong to time and frequency domains, and the learning phase relies on training sequences. All the aforementioned studies lack theoretical models that relate the data collected with the number of targets, preventing the design of solid and accurate crowd-centric techniques.

The fundamental questions related to target counting are: (i) how is the number of targets related to observed data? (ii) is there any observable feature that can be described as a function of the number of targets? The answers to these questions enable the design of low-complexity crowd-centric techniques for device-free target counting. The goal of this paper is to develop a device-free counting method based on information extracted from the wireless waveforms received after target backscattering.

This paper develops a framework for the design of counting systems. First, the counting problem is formalized by relying on model order selection, which requires target localization. The related individual-centric method based on Bayesian estimation is derived. Then, a crowd-centric method that relies on energy detection is proposed. The key idea is to consider the geometrical relation between the target position and the energy samples, at the output of the energy detection. Differently from other papers in the literature, a tractable theoretical model is provided for describing the relation between the number of targets and the energy samples for wideband signals. The key contributions of this paper can be summarized as follows:

- formalization of the counting problem through model order selection;
- development of a framework that relates the target counting problem to the energy detection output;
- proposal of low-level features for crowd-centric counting and a tractable observation model for wideband signals;
- quantification of performance metrics in a use case and comparison with existing methods.

The remaining sections are organized as follows. Sec. II describes the system model. Sec. III devises the individual-centric and crowd-centric counting systems. Sec. IV presents the counting problem as a model order selection related to target localization. Sec. V introduces the energy-based crowd-counting and the corresponding tractable model for wideband signals. Sec. VI describes a case study and numerical results. Finally, in Sec. VII our conclusions are given.

Notation: Random variables are displayed in sans serif, upright fonts; their realizations in serif, italic fonts. Vectors are denoted by bold lowercase letters. For example, a random variable (RV) and its realization are denoted by x and x; a random vector and its realization are denoted by $\mathbf{x}$ and $\boldsymbol{x}$. Sets and random sets are denoted by upright sans serif and calligraphic font, respectively. For example, a random set and its realization are denoted by X and $\mathcal{X}$, respectively. The $\emptyset$ denotes the empty set. The main symbols used throughout the paper are reported in Table I.

TABLE I
MAIN SYMBOLS USED THROUGHOUT THE PAPER

Symbol	Description
n_{p}	number of transmitter-receiver pairs
$\mathcal{N}_{\mathrm{p}}$	index set of transmitter-receiver pairs
$\boldsymbol{p}_{\mathrm{tx}}^{(i)}$	position of the ith transmitter
$\boldsymbol{p}_{\mathrm{rx}}^{(i)}$	position of the ith receiver
$s(t)$	transmitted signal
N_{t}	index set of targets
n_{t}	number of targets
$\mathbf{p}_{\mathsf{t}}^{(k)}$	position of the kth target
$\mathbf{p}_{\mathsf{b}}^{(k)}$	position of the kth background object
$\mathsf{r}^{(i)}(t)$	signal received at the ith receiver
$\mathsf{r}_{\mathsf{b}}^{(i)}(t)$	component of $\mathsf{r}^{(i)}(t)$ related to the background
$\mathsf{r}_{\mathsf{t}}^{(i)}(t)$	component of $\mathsf{r}^{(i)}(t)$ related to the targets
$\mathsf{n}^{(i)}(t)$	noise component of $\mathsf{r}^{(i)}(t)$
$\mathsf{M}_k^{(i)}$	index set of multipath components for the kth cluster
$\boldsymbol{\alpha}_{k,m}^{(i)}$	amplitude of the mth component for the kth cluster
$\mathsf{t}_k^{(i)}$	arrival time for the kth cluster in $\mathsf{r}^{(i)}(t)$
$\boldsymbol{\tau}_{k,m}^{(i)}$	excess delay of the mth component for the kth cluster
$\hat{r}_{\mathsf{b}}^{(i)}(t)$	estimation of $\mathsf{r}_{\mathsf{b}}^{(i)}(t)$
$\tilde{\mathsf{r}}^{(i)}(t)$	signal at the ith receveir after background removal
$\tilde{\mathbf{r}}$	concatenation of vectors of received signal samples
$\mathbf{p}_{\mathsf{t}}$	concatenation of the target position vectors
$n_{\max}$	maximum number of targets
$\mathcal{H}_n$	hypothesis that the number of targets is $n_{\mathsf{t}} = n$
$f(\tilde{\mathbf{r}}\|\mathcal{H}_{\mathsf{n}_{\mathsf{t}}})$	likelihood function for the nth hypothesis
$f(\tilde{\mathbf{r}}, \mathbf{p}_{\mathsf{t}})$	likelihood function for the position vector $\mathbf{p}_{\mathsf{t}}$
$\mathcal{P}_n$	set of possible $\mathbf{p}_{\mathsf{t}}$ composed of n position vectors
$\hat{\mathsf{n}}_{\mathsf{t}}$	estimated number of targets
$\mathbf{f}$	observable feature
$h(\cdot)$	extraction function
$g(\cdot)$	observation function
e_{rms}	root-mean-square of the counting error
P_{ceo}	counting error outage
$\boldsymbol{\theta}^{(i)}$	ith vector of target positions, amplitudes, and delays
$\tilde{f}(\mathbf{r}\|\mathbf{p}_{\mathsf{t}})$	approximated likelihood function
T_{d}	dwell time of the energy detector
$\mathsf{e}_k^{(i)}$	kth energy bin for the ith signal
$\mathbf{e}^{(i)}$	vector of energy bin for the ith signal
$\boldsymbol{\lambda}_k^{(i)}$	non-centrality parameter for $\mathsf{e}_k^{(i)}$
$\mathcal{E}_k^{(i)}$	kth elliptical region defined by $\mathsf{e}_k^{(i)}$
$\mathsf{N}_k^{(i)}$	number of targets in $\mathcal{E}_k^{(i)}$

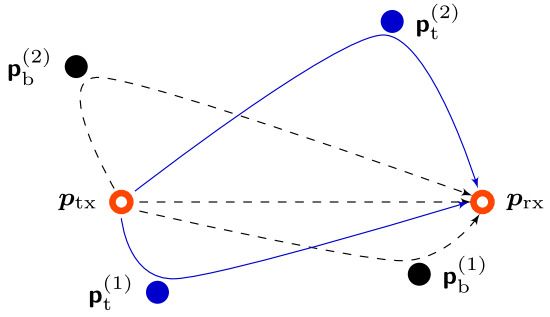

Fig. 1. A bistatic sensor radar. Red empty circles represent the transmitter and receiver positions, blue circles represent the target scatterers, and black circles represent the background scatterers. Black dashed lines indicate the direct path between the transmitter and receiver as well as the first multipath component related to the background scatterers. Blue solid lines indicate the first multipath component related to the background scatterers.

II. System Model

Consider a network of n_{p} transmitter-receiver pairs operating as sensor radars (SRs), with index set $\mathcal{N}_{\mathrm{p}} = \{1, 2, \ldots, n_{\mathrm{p}}\}$.[1] The transmitter of the ith pair is in position $\boldsymbol{p}_{\mathrm{tx}}^{(i)}$ and emits a signal $s(t)$; the receiver is in position $\boldsymbol{p}_{\mathrm{rx}}^{(i)}$ and collects the received signal after backscattering by all the objects in the operating environment, also referred to as scatterers.

Consider a random set $\mathsf{N_t}$ of $\mathsf{n_t}$ targets, where the kth target is located in position $\mathbf{p}_{\mathrm{t}}^{(k)}$ with $k \in \mathsf{N_t}$, and a random set $\mathsf{N_b}$ of $\mathsf{n_b}$ background objects in position $\mathbf{p}_{\mathrm{b}}^{(k)}$ with $k \in \mathsf{N_b}$.[2] In particular, the background objects are those present in the environment even in the absence of targets (i.e., prior knowledge on their positions is available). Fig. 1 shows an example of bistatic SR (i.e., one transmitter and one receiver), with two target scatterers and two background scatterers.

The emitted signal propagates according to the Saleh-Valenzuela channel model [35] where the multipath clusters are related to objects (named super scatterers) which are randomly located in the operating environment [36]–[39]. In particular, multiple reflection points of the same super-scatterer lead to different multipath components within the corresponding cluster. The randomness of object positions and of the reflecting point locations on the scatterers' surface lead to the double Poisson processes that describe the arrival time of clusters and multipath components [36].

As a result, the equivalent low-pass signal gathered by the receiver of the ith pair after multipath propagation can be expressed as

$$\mathsf{r}^{(i)}(t) = \mathsf{r}_{\mathrm{b}}^{(i)}(t) + \mathsf{r}_{\mathrm{t}}^{(i)}(t) + \mathsf{n}^{(i)}(t) \tag{1}$$

where the component related to the targets is given by

$$\mathsf{r}_{\mathrm{t}}^{(i)}(t) = \sum_{k \in \mathsf{N_t}, m \in \mathsf{M}_k^{(i)}} \boldsymbol{\alpha}_{k,m}^{(i)} s(t - \mathsf{t}_k^{(i)} - \boldsymbol{\tau}_{k,m}^{(i)}) \tag{2}$$

and that related to the background scatterers (in addition to the transmitter-receiver path) is given by

$$\begin{aligned}\mathsf{r}_{\mathrm{b}}^{(i)}(t) =& \boldsymbol{\alpha}_0^{(i)} s(t - \|\boldsymbol{p}_{\mathrm{tx}}^{(i)} - \boldsymbol{p}_{\mathrm{rx}}^{(i)}\|/c) \\ &+ \sum_{k \in \mathsf{N_b}} \sum_{m \in \mathsf{M}_k} \boldsymbol{\alpha}_{k,m}^{(i)} s(t - \mathsf{t}_k^{(i)} - \boldsymbol{\tau}_{k,m}^{(i)}),\end{aligned} \tag{3}$$

$\mathsf{n}^{(i)}(t)$ denotes the zero-mean Gaussian distributed noise component with variance σ_{n}^2, $\mathsf{M}_k^{(i)}$ is the index set of multipath components in the kth cluster, with random cardinality $\mathsf{m}_k^{(i)}$, $\mathsf{t}_k^{(i)} = \|\boldsymbol{p}_{\mathrm{tx}}^{(i)} - \mathbf{p}_{\mathrm{t}}^{(k)}\|/c - \|\mathbf{p}_{\mathrm{t}}^{(k)} - \boldsymbol{p}_{\mathrm{rx}}^{(i)}\|/c$, $\boldsymbol{\tau}_{k,m}^{(i)}$ is the excess arrival delay of the mth component in the kth cluster with amplitude $\boldsymbol{\alpha}_{k,m}^{(i)}$.[3] The expected value of $\boldsymbol{\alpha}_{k,m}^{(i)}$ averaged over small-scale fading is

$$\overline{\boldsymbol{\alpha}}_k^{(i)} = \mathbb{E}\left\{\boldsymbol{\alpha}_{k,m}^{(i)}\right\} = \mathsf{Q}_{\mathrm{k}}^{(i)} \exp(\mathsf{t}_k^{(i)}/\gamma^{(i)}) \tag{4}$$

where

$$\mathsf{Q}_k^{(i)} = \frac{10^{\mathsf{P}_k^{(i)}/10}}{\sum_{k=1}^{\mathsf{n_t}} \mathsf{t}_k^{(i)}/\gamma^{(i)}}, \tag{5}$$

$\gamma^{(i)}$ is the power decay constant, and $\mathsf{P}_k^{(i)}$ is the average received signal strength (RSS) for a target at $\mathbf{p}_{\mathrm{t}}^{(i)}$ with respect to the ith pair, i.e., considering the path-loss and the radar cross section (RCS) of the corresponding scatterer [21], [27], [39].[4]

A temporal separation between two signal replicas is necessary to ensure their resolvability, which results in a minimum resolvable delay that depends on the transmitted signal and the receiver bandwidth [21]. Therefore, for counting systems the use of wideband and UWB signals is preferable to that of narrowband signals thanks to the better path delay resolvability, which is crucial to distinguish between different scatterers.

The background signal $\mathsf{r}_{\mathrm{b}}^{(i)}(t)$ can be measured offline in the absence of any target. Let $\hat{r}_{\mathrm{b}}^{(i)}(t)$ be the estimated background component which represents the prior knowledge on the operating environment. The background estimate can be removed from the received waveform leading to $\tilde{\mathsf{r}}^{(i)}(t) = \mathsf{r}^{(i)}(t) - \hat{r}_{\mathrm{b}}^{(i)}(t)$, which is the received signal after background removal. The aim of the counting system is to process the signal $\tilde{\mathsf{r}}^{(i)}(t)$ for counting the number of target scatterers $\mathsf{n_t}$.

III. Individual-centric and Crowd-centric Counting Methods

Consider the concatenation of vectors composed of the received signal samples, after background removal, for each transmitter-receiver pair

$$\tilde{\mathbf{r}} = \left[\tilde{\mathbf{r}}^{(1)}, \tilde{\mathbf{r}}^{(2)}, \ldots, \tilde{\mathbf{r}}^{(n_{\mathrm{p}})}\right]. \tag{6}$$

[1]The following analysis holds either in the multistatic configuration, i.e., the transmitter and receiver of each pair are in different positions, and in the monostatic configuration, i.e., the transmitter and receiver of each pair are co-located.

[2]Note that scatterer positions are random vectors, the number of scatterers is a random variable, whereas transmitter and receiver positions are deterministic and known.

[3]Note that the first component of the sum in (3) is related to the direct path between the transmitter and receiver, with amplitude $\boldsymbol{\alpha}_0^{(i)}$.

[4]The RCS measures the power density that the object reflects with respect to the incident power, in relation to scatterer orientation, material, and size [22], [27], [40].

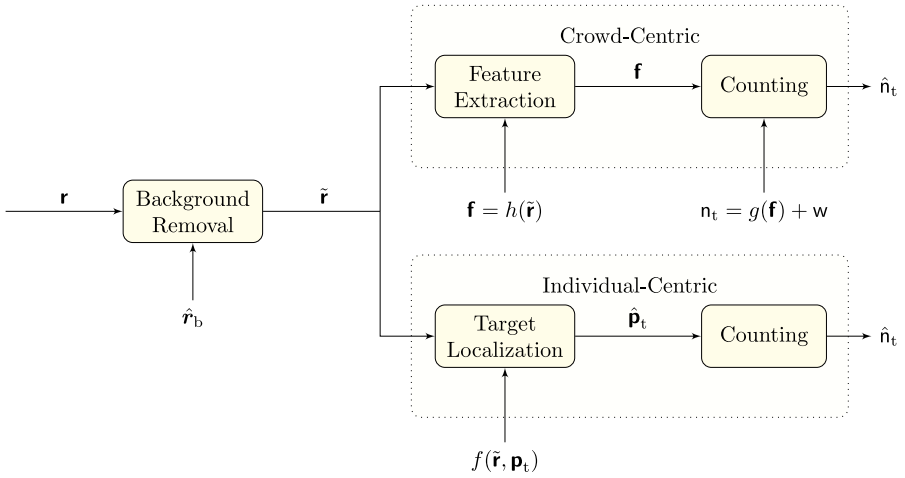

Fig. 2. Illustration of the signal processing of the individual-centric and crowd-centric methods for target counting.

The number of samples in the vector $\tilde{\mathbf{r}}$ is $n_\mathrm{p}\, n_\mathrm{s}$, where n_s is the number of received signal samples in $\tilde{\mathbf{r}}^{(i)}$, which depends on the observation interval T_obs and the sampling time T_s, i.e., $n_\mathrm{s} = \lfloor T_\mathrm{obs}/T_\mathrm{s} \rfloor$, where $\lfloor x \rfloor$ is the largest integer less than or equal to x. The vector

$$\mathbf{p}_\mathrm{t} = \left[\mathbf{p}_\mathrm{t}^{(1)}, \mathbf{p}_\mathrm{t}^{(2)}, \ldots, \mathbf{p}_\mathrm{t}^{(\mathsf{n}_\mathrm{t})}\right] \tag{7}$$

represents the concatenation of the target position vectors. Fig. 2 illustrates the block diagram for the individual-centric and crowd-centric counting methods starting from the vector of received signal samples $\mathbf{r}$.

A. Individual-Centric Method

The individual-centric method relies on the data model that relates $\tilde{\mathbf{r}}$ and $\mathbf{p}_\mathrm{t}$, and can be performed via classic multi-target detection algorithms [21], [22]. First, the targets are localized and then an estimate of the number of targets $\hat{\mathsf{n}}_\mathrm{t}$ is determined from the length of the estimated vector $\hat{\mathbf{p}}_\mathrm{t}$. This corresponds to a model order selection problem: the estimation of an integer value that is the dimension of the parameter vector of a data model [41].

Let $\mathcal{H}_n$ denote the hypothesis that $\mathsf{n}_\mathrm{t} = n$, and let n_max denote a known upper bound for n_t, i.e., $\mathsf{n}_\mathrm{t} \in \mathcal{N} = \{1, 2, \ldots, n_\mathrm{max}\}$. The aim of the system is to estimate n_t from $\tilde{\boldsymbol{r}}$ as the maximum likelihood (ML) estimate

$$\hat{\mathsf{n}}_\mathrm{t} = \underset{n \in \mathcal{N}}{\operatorname{argmax}}\, f(\tilde{\boldsymbol{r}}|\mathcal{H}_n). \tag{8}$$

Therefore, the hypothesis $\mathcal{H}_n$, i.e., $\mathsf{n}_\mathrm{t} = n$, is true for any target position $\mathbf{p}_\mathrm{t}$ with length $d\,n$, where $\mathbf{p}_\mathrm{t}^{(i)} \in \mathbb{R}^d \;\; \forall i = 1, 2, \ldots, n$. A Bayesian approach is considered, where the density function $f(\tilde{\mathbf{r}}, \mathbf{p}_\mathrm{t})$ is marginalized over the space $\mathcal{P}_n = \{\mathbf{p}_\mathrm{t} : \mathsf{n}_\mathrm{t} = n\}$, i.e.[5]

$$f(\tilde{\mathbf{r}}|\mathcal{H}_n) = \int_{\mathcal{P}_n} f(\tilde{\mathbf{r}}, \mathbf{p}_\mathrm{t})\, d\mathbf{p}_\mathrm{t}\,. \tag{9}$$

[5]The following analysis can be extended to the case of dynamic targets by considering Bayesian filtering over time, i.e., multi-target tracking [21], [22].

Such a density function can be asympthotically approximated with respect to n, leading to different information criteria [41].[6] The most adopted asymptotic approximation for (8) is based on the ML estimation

$$\begin{aligned}\hat{\mathsf{n}}_\mathrm{t} &= \underset{n \in \mathcal{N}}{\operatorname{argmax}}\, f(\tilde{\boldsymbol{r}}|\mathcal{H}_n) \\ &= \underset{n \in \mathcal{N}}{\operatorname{argmax}} \max_{\mathbf{p}_\mathrm{t} \in \mathcal{P}_n} f(\tilde{\boldsymbol{r}}, \mathbf{p}_\mathrm{t})\,.\end{aligned} \tag{10}$$

The derivation of $f(\tilde{\mathbf{r}}, \mathbf{p}_\mathrm{t})$ for wideband signals is presented in Sec. IV.

B. Crowd-Centric Method

The crowd-centric method relies on a vector of observable features $\mathbf{f}$. For example, features can be related to the envelope of the received signal and the shape of its energy samples. The vector $\mathbf{f}$ is obtained from $\tilde{\mathbf{r}}$ through a feature extraction function h, i.e.,

$$\mathbf{f} = h(\tilde{\mathbf{r}}) \tag{11}$$

and is related to n_t through an observation model[7]

$$\mathsf{n}_\mathrm{t} = g(\mathbf{f}) + \mathsf{w} \tag{12}$$

where g is the observation function and w is the measurement noise. The choice of features $\mathbf{f}$ is crucial for the counting performance, despite $g(\mathbf{f})$ and the distribution of the measurement noise w are unknown in general. A new energy-based feature and its observation model are introduced for wideband systems in Sec. V.

[6]An alternative to the Bayesian approach is to obtain $\hat{\mathsf{n}}_\mathrm{t}$ by minimizing the Kullback-Leibler divergence between the true probability distribution function (PDF) of the observed data and the one of the model. If the PDF of the model is not available in closed form, different approximation can be considered, leading to the Akaike and generalized information criteria [41].

[7]The following analysis can be extended to the case of dynamic targets by deriving a transition function that relates the number of targets at time t with the number of targets at time $t + \delta t$ [21], [22].

C. Counting Complexity

We now consider the counting complexity for the individual-centric and crowd-centric methods. The complexity of the individual-centric method is equal to that of the multi-target detection problem, which is NP-hard and depends on the maximum number of hypotheses $n_{\max}$ [21], [22], [42]. In general, (9) and (10) require to compare $f(\tilde{\mathbf{r}}, \mathbf{p}_\mathsf{t})$ for every value of $\mathbf{p}_\mathsf{t} \in \mathcal{P}_n$ and every $\mathsf{n} \in \mathcal{N}$. For a grid-based algorithm with n_g possible positions (i.e., $\mathcal{P}_1$ is a finite set with cardinality $|\mathcal{P}_1| = n_\mathrm{g}$) the number of comparisons is $\sum_{i=0}^{n_{\max}} \binom{n_\mathrm{g}}{i}$. For example, if $n_\mathrm{g} = n_{\max}$, the number of comparisons is $2^{n_{\max}}$.

The complexity of the crowd-centric method depends on the feature extraction function h and on the observation function g, while it is independent of the number of targets. For the case study presented in Sec. VI, the running time T_IC of the individual-centric algorithm was $T_\mathrm{IC} = 13.5\, T_\mathrm{CC}$ for $n_{\max} = 5$, and $T_\mathrm{IC} = 406\, T_\mathrm{CC}$ for $n_{\max} = 10$, where T_CC was the running time for the crowd-centric algorithm proposed in this paper.[8]

Remark 1: The crowd-centric method significantly reduces the computational complexity with respect to that of the individual-centric. In addition, the complexity of the crowd-centric method does not depend on the number of targets.

IV. Individual-centric Counting via Wideband Signals

The individual-centric method requires the derivation of $f(\tilde{\mathbf{r}}, \mathbf{p}_\mathsf{t})$ to calculate $f(\tilde{\mathbf{r}}|\mathcal{H}_n)$.

A. Likelihood Function

From (1), (2), and (3), if the background is perfectly removed,[9] i.e., $\hat{r}_\mathrm{b}^{(i)}(t) = r_\mathrm{b}^{(i)}(t)$, then $\tilde{\boldsymbol{r}}^{(i)}$ is the realization of a random vector $\tilde{\mathbf{r}}^{(i)}$ that depends on a parameter vector $\boldsymbol{\theta}^{(i)} = [\mathbf{p}_\mathsf{t}, \boldsymbol{\tau}^{(i)}, \boldsymbol{\alpha}^{(i)}]$, where[10]

$$\begin{aligned}\boldsymbol{\tau}^{(i)} &= [\tau_{1,1}^{(i)}, \tau_{1,2}^{(i)}, \ldots, \tau_{1,\mathsf{m}_1^{(i)}}^{(i)}, \ldots, \tau_{k,1}^{(i)}, \ldots, \tau_{\mathsf{n}_\mathsf{t},\mathsf{m}_{\mathsf{n}_\mathsf{t}}^{(i)}}^{(i)}] \\ \boldsymbol{\alpha}^{(i)} &= [\alpha_{1,1}^{(i)}, \alpha_{1,2}^{(i)}, \ldots, \alpha_{1,\mathsf{m}_1^{(i)}}^{(i)}, \ldots, \alpha_{k,1}^{(i)}, \ldots, \alpha_{\mathsf{n}_\mathsf{t},\mathsf{m}_{\mathsf{n}_\mathsf{t}}^{(i)}}^{(i)}]. \end{aligned} \quad (13)$$

The parameters in $\boldsymbol{\tau}^{(i)}$ and $\boldsymbol{\alpha}^{(i)}$ (i.e., the excess delays and amplitudes of the multipath components within each cluster) are RVs that depend on the channel instantiation.[11]

Since the received waveforms from different transmitter-receiver pairs are independent, the likelihood function is

$$f(\tilde{\mathbf{r}}, \mathbf{p}_\mathsf{t}) \propto \prod_{i \in \mathcal{N}_\mathrm{p}} f(\tilde{\mathbf{r}}^{(i)}|\mathbf{p}_\mathsf{t}). \quad (14)$$

The PDF $f(\tilde{\mathbf{r}}^{(i)}|\mathbf{p}_\mathsf{t})$ can be obtained as marginal distribution

$$f(\tilde{\mathbf{r}}^{(i)}|\mathbf{p}_\mathsf{t}) = \mathbb{E}_{\boldsymbol{\alpha}^{(i)},\boldsymbol{\tau}^{(i)}}\Big\{ f(\tilde{\mathbf{r}}^{(i)}|\boldsymbol{\theta}^{(i)}) \Big\} \quad (15)$$

where the marginalization has been made with respect to $\boldsymbol{\alpha}^{(i)}$ and $\boldsymbol{\tau}^{(i)}$. Specifically,

$$\begin{aligned} f(\tilde{\mathbf{r}}^{(i)}|\boldsymbol{\theta}^{(i)}) \propto \exp\Big\{ & 2 \int_0^{T_\mathrm{obs}} \tilde{r}^{(i)}(t) \sum_{k \in \mathsf{N}_\mathsf{t}, m \in \mathsf{M}_k^{(i)}} \alpha_{k,m}^{(i)} s(t - \mathsf{t}_k^{(i)} - \tau_{k,m}^{(i)}) dt \\ & - \int_0^{T_\mathrm{obs}} \Big[\sum_{k \in \mathsf{N}_\mathsf{t}, m \in \mathsf{M}_k^{(i)}} \alpha_{k,m}^{(i)} s(t - \mathsf{t}_k^{(i)} - \tau_{k,m}^{(i)}) \Big]^2 dt \Big\} \end{aligned} \quad (16)$$

is the PDF for a given channel instantiation.

The excess delays $\tau_{k,m}^{(i)}$ of multipath components depend on the environment, the specific target, and the orientation, all of which are unknown. Therefore, the marginalization with respect to the channel parameter may be impossible or lead to intractable problems. This calls for approximations to obtain tractable models [26].

B. Tractable Likelihood Function

Consider a single-bounce channel, where each scatterer introduces one resolvable multipath component at the receiver, with arrival time and amplitude determined by the target position [36]. In particular, the amplitude is averaged over small-scale fading as in (4). The single-bounce model is realistic in the presence of bandwidth limitations, which are intrinsic to hardware and signal processing, because multiple reflection from the same target cannot be resolved at the receiver. Following the single-bounce mode, the likelihood function is found to be

$$\begin{aligned} f(\tilde{\mathbf{r}}^{(i)}|\boldsymbol{\theta}^{(i)}) &\simeq \tilde{f}(\tilde{\mathbf{r}}^{(i)}|\mathbf{p}_\mathsf{t}) \\ &\propto \exp\Big\{ 2 \int_0^{T_\mathrm{obs}} \tilde{r}^{(i)}(t) \sum_{k \in \mathsf{N}_\mathsf{t}} \overline{\alpha}_{k,1}^{(i)} s(t - \mathsf{t}_k^{(i)}) dt \\ &\quad - \int_0^{T_\mathrm{obs}} \Big[\sum_{k \in \mathsf{N}_\mathsf{t}} \overline{\alpha}_{k,1}^{(i)} s(t - \mathsf{t}_k^{(i)}) \Big]^2 \Big\}. \end{aligned} \quad (17)$$

Fig. 3(a) shows an example of likelihood function for the case $\mathsf{N}_\mathsf{t} = \{1, 2\}$ as a function of $\mathbf{p}_\mathsf{t}^{(2)}$ when $\mathbf{p}_\mathsf{t}^{(1)} = \boldsymbol{p}_\mathsf{t}^{(1)}$ and the channel instantiation is known (ideal case). It can be noticed that the contour plot of the likelihood function approximately forms an elliptical ring, having foci at the transmitter and receiver location, passing through the real position of $\mathbf{p}_\mathsf{t}^{(2)}$.[12] The size of the ring is related to the uncertainty of the position due to the noise variance. Fig. 3(b) shows the approximated version of the likelihood when a single-bounce model is used for the likelihood function. It can be observed that the uncertainty increases with respect to the ideal case and the shape is more irregular, but the elliptical ring maintains the same foci and the maximum value that includes the true position of $\mathbf{p}_\mathsf{t}^{(2)}$.

[8] Simulations were conducted in Matlab R2016b 64-bit floating point precision.

[9] In the case of imperfect background removal, our derivations hold by considering the positions of the unknown background objects as RVs in the likelihood function.

[10] We consider zero-mean gaussian distributed noise samples $n_j^{(i)} = n^{(i)}(t_j) \sim \mathcal{N}(0, \sigma_\mathrm{n}^2)$ and the variance σ_n^2 is considered known to simplify the notation.

[11] Note that the cluster arrival time is a function of by $\mathbf{p}_\mathsf{t}$, in the following considered uniformly distributed in $\mathcal{P}_{\mathsf{n}_\mathsf{t}}$.

[12] It is known from radar theory that the likelihood function defines isorange contours that are circumferences or ellipses in the monostatic and bistatic case, respectively [21].

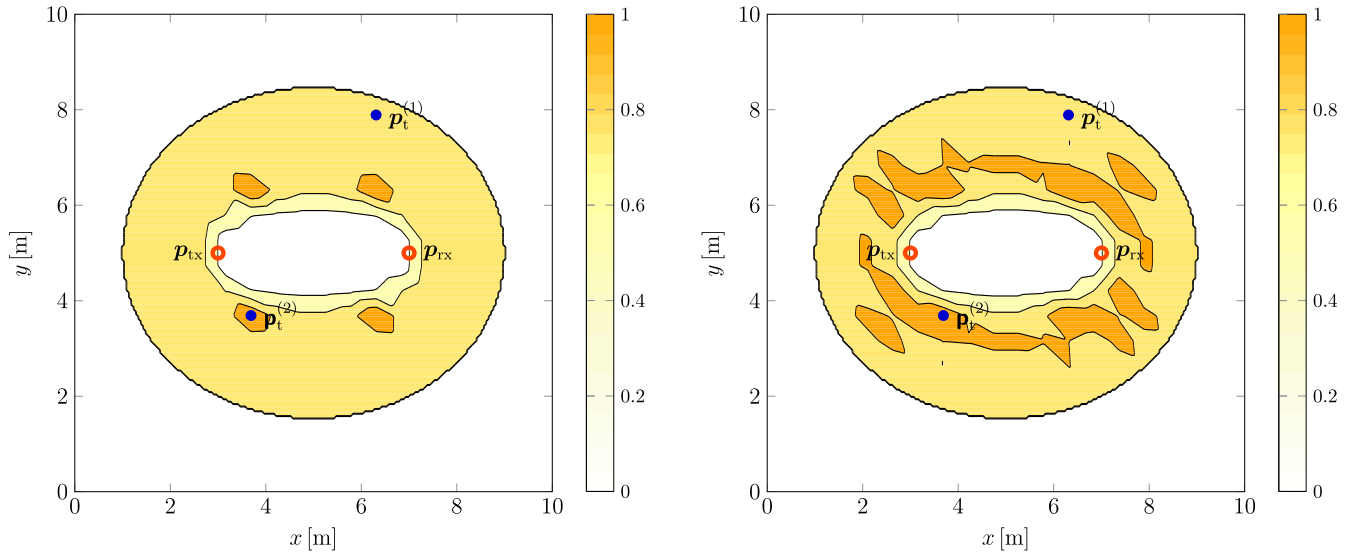

(a) $f(\tilde{\boldsymbol{r}}^{(1)}, \mathbf{p}_t^{(2)} | \mathbf{p}_t^{(1)} = \boldsymbol{p}_t^{(1)}, \boldsymbol{\alpha})$ (b) $\tilde{f}(\tilde{\boldsymbol{r}}^{(1)}, \mathbf{p}_t^{(2)} | \mathbf{p}_t^{(1)} = \boldsymbol{p}_t^{(1)}, \overline{\boldsymbol{\alpha}})$

Fig. 3. Contour plot of $f(\tilde{\boldsymbol{r}}^{(1)}, \mathbf{p}_t^{(2)} | \mathbf{p}_t^{(1)} = \boldsymbol{p}^{(1)}, \boldsymbol{\alpha})$ and its single-bounce approximation $\tilde{f}(\tilde{\boldsymbol{r}}^{(1)}, \mathbf{p}_t^{(2)} | \mathbf{p}_t^{(1)} = \boldsymbol{p}_t^{(1)}, \overline{\boldsymbol{\alpha}})$ for a given realization $\tilde{\mathbf{r}}^{(1)} = \tilde{\boldsymbol{r}}^{(1)}$ varying $\mathbf{p}_t^{(2)}$, plotted for $0 < \|\boldsymbol{p}_{tx} - \mathbf{p}_t^{(2)}\| + \|\mathbf{p}_t^{(2)} - \boldsymbol{p}_{rx}\| \leq 8$ m. The color indicates the likelihood value from lighter (low values) to darker (high values).

By applying the single-bounce model to (9), the model order selection problem can be expressed as

$$\begin{aligned} \hat{n}_t &= \underset{n \in \mathcal{N}}{\operatorname{argmax}}\, f(\tilde{\mathbf{r}} | \mathcal{H}_n) \\ &\simeq \underset{n \in \mathcal{N}}{\operatorname{argmax}} \int_{\mathcal{P}_n} \tilde{f}(\mathbf{r} | \mathbf{p}_t)\, d\mathbf{p}_t \end{aligned} \tag{18}$$

where $\mathcal{H}_n$ is considered true for any $\mathbf{p}_t \in \mathcal{P}_n$ and $\mathbf{p}_t$ is uniformly distributed in $\mathcal{P}_n$.

V. Crowd-Centric Counting via Wideband Signals

We now propose a crowd-centric method based on energy detection by providing the extraction and observation functions.

A. Energy Detection

Energy detection is widely adopted for ranging [43]–[46], spectrum sensing [47]–[49], and carrier sensing [50]–[52]. Fig. 4(a) illustrates the energy detection scheme, which takes as input the received signal after background removal, $\tilde{\mathsf{r}}^{(i)}(t)$, and calculates a vector of energy bins $\mathbf{e}^{(i)}$ that is processed for counting. The signal is sampled by an analog to digital converter (A/D) with sampling time T_s. The observation time interval $(0, T_{obs}]$ is divided into time intervals (bins) of duration T_d (dwell time),[13] leading to a total of $n_{bin} = \lfloor T_{obs}/T_d \rfloor$ bins. The kth bin spans the signal samples $\tilde{\mathsf{r}}^{(i)}(t_j)$ with $t_j \in \mathcal{T}_k = ((k-1)T_d, kT_d]$. The energy sample associated with the kth bin is a RV obtained through a quadrature integration and dump (QID) as

$$\mathsf{e}_k^{(i)} = \sum_{t_j \in \mathcal{T}_k} \tilde{\mathsf{r}}^2(t_j) \tag{19}$$

where $t_j = t_{j-1} + T_s$ in which $j = 1, 2, \ldots, n_{sb}$, and n_{sb} is the number of samples per bin. Therefore, the number of samples contained in a time bin is $n_{sb} = \lfloor T_d/T_s \rfloor$. The output of the energy detector is the energy bin vector $\mathbf{e}^{(i)} = [\mathsf{e}_1^{(i)}, \mathsf{e}_2^{(i)}, \ldots, \mathsf{e}_{n_{bin}}^{(i)}]$.

The geometrical interpretation of the energy bin vector is described by defining n_{bin} regions $\mathcal{E}_k^{(i)} \subset \mathbb{R}^d$ with $k = 1, 2, \ldots, n_{bin}$ for the ith transmitter-receiver pair as

$$\mathcal{E}_k^{(i)} = \left\{ \boldsymbol{p} \in \mathbb{R}^d \text{ s.t. } (\|\boldsymbol{p} - \boldsymbol{p}_{tx}^{(i)}\| + \|\boldsymbol{p} - \boldsymbol{p}_{rx}^{(i)}\|)/c \in \mathcal{T}_k \right\}. \tag{20}$$

The region $\mathcal{E}_k^{(i)}$ is the locus of points $\boldsymbol{p} \in \mathbb{R}^d$ such that the signal emitted by the ith transmitter and backscattered by a target at $\boldsymbol{p}$ arrives at the ith receiver with a TOA τ that falls into the kth bin (i.e., $(k-1)T_d < \tau \leq kT_d$). In particular, $\mathcal{E}_k^{(i)}$ is an elliptical ring when $d = 2$ with foci at the ith transmitter and receiver positions (see Fig. 4(b)).

For the ith target-receiver pair, the set

$$\mathsf{N}_k^{(i)} = \{ j \in \mathsf{N}_t \text{ s.t } \boldsymbol{p}_t^{(j)} \in \mathcal{E}_k^{(i)} \} \tag{21}$$

is the index set of target scatterers lying inside the region $\mathcal{E}_k^{(i)}$. As the bins, thus the region are non-overlapping and[14]

$$\mathsf{N}_t = \bigcup_{k=1}^{n_{bin}} \mathsf{N}_k^{(i)} \ \forall i = 1, 2, \ldots, n_p. \tag{22}$$

Each element $\mathsf{e}_k^{(i)}$ of the energy bin vector is distributed according to a chi-square RV conditional on the channel instantiation. In particular, given $\boldsymbol{\tau}^{(i)}$ and $\boldsymbol{\alpha}^{(i)}$, the $\mathsf{e}_k^{(i)}/\sigma_n^2 \sim \chi_{n_{sb}}(\lambda_k^{(i)})$, i.e., a non-central chi-square RV with n_{sb} degrees

[13]The dwell time T_d represents the time resolution at the output of the energy detector.

[14]To simplify the notation, here we assume that every transmitter-receiver pair detects all the targets.

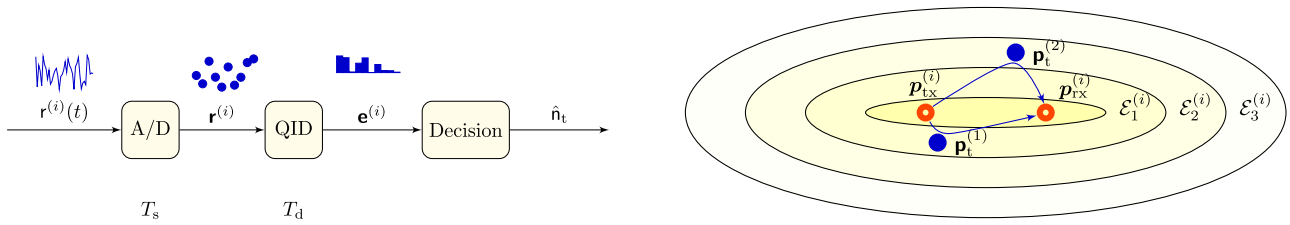

(a) Energy detection scheme for counting.

(b) Example of elliptical regions for n_{bin}=3, $\mathsf{N}_\text{t} = \{1, 2\}$, $\mathsf{N}_1 = \{1\}$, $\mathsf{N}_2 = \{2\}$, and $\mathsf{N}_3 = \emptyset$.

Fig. 4. Illustration of the energy detection scheme and of the geometrical representations of the time intervals in elliptical regions.

of freedom and non-centrality parameter $\lambda_k^{(i)}$ [26], [43], [53]–[56]. The non-centrality parameter $\lambda_k^{(i)}$ depends on $\boldsymbol{\theta}^{(i)} = [\mathbf{p}_\text{t}, \boldsymbol{\tau}^{(i)}, \boldsymbol{\alpha}^{(i)}]$ and is given by

$$\begin{aligned}\lambda_k^{(i)} &= \frac{1}{\sigma_\text{n}^2} \sum_{t_j \in \mathcal{T}_k} \tilde{\mathsf{r}}_\text{t}^{(i)}(t_j)^2 \\ &= \frac{1}{\sigma_\text{n}^2} \sum_{t_j \in \mathcal{T}_k} \Big[\sum_{k \in \mathsf{N}_\text{t}} \sum_{m \in \mathsf{M}_k^{(i)}} \alpha_{k,m}^{(i)} s(t_j - \mathsf{t}_k^{(i)} - \tau_{k,m}^{(i)}) \Big]^2 .\end{aligned} \tag{23}$$

B. Feature Extraction Function

By expanding the square of the double summation in (23) we obtain

$$\begin{aligned}\tilde{\mathsf{r}}_\text{t}^{(i)}(t_j)^2 = &\sum_{l \in \mathsf{M}^{(i)}} (\check{\alpha}_l^{(i)})^2 s^2(t_j - \check{\tau}_l^{(i)}) \\ &+ \sum_{h \in \mathsf{M}^{(i)}} \sum_{u<h} \check{\alpha}_h^{(i)} \check{\alpha}_u^{(i)} s(t_j - \check{\tau}_h^{(i)}) s(t_j - \tau_u^{(i)})\end{aligned} \tag{24}$$

where $\mathsf{M}^{(i)} = \cup_{k=1}^{n_\text{t}} \mathsf{M}_k^{(i)}$, $\check{\alpha}_l^{(i)} = \alpha_{k,m}^{(i)}$ and $\check{\tau}_l^{(i)} = \mathsf{t}_k^{(i)} + \tau_{k,m}^{(i)}$, with $l = \mathsf{m}_k^{(i)}(k-1) + l$.

We noticed that the feature $\mathsf{f}_k^{(i)} = \lambda_k^{(i)}$ can be extracted from $\mathbf{e}^{(i)}$ and is related to n_t through (23). In particular, since $\mathbb{E}\left\{\mathsf{e}_k^{(i)}/\sigma_\text{n}^2\right\} = n_\text{sb} + \lambda_k^{(i)}$ then the extraction function for the ith pair in the kth time interval is

$$\mathsf{f}_k^{(i)} = h(\tilde{\mathbf{r}}^{(i)}) = \frac{\mathsf{e}_k^{(i)}}{\sigma_\text{n}^2} - n_\text{sb} \,. \tag{25}$$

The ensemble of $\mathsf{f}_k^{(i)}$ forms the vector $\mathbf{f} = [\mathsf{f}_1^{(1)}, \mathsf{f}_2^{(1)}, \ldots, \mathsf{f}_{n_\text{bin}}^{(1)}, \mathsf{f}_1^{(2)}, \ldots, \mathsf{f}_{n_\text{bin}}^{(n_\text{p})}]$ of length $n_\text{bin}\, n_\text{p}$. The observation model $\mathsf{n}_\text{t} = g(\mathsf{f}_k^{(i)}) + \mathsf{w}$ would be obtained by inverting (23) with respect to n_t. However, such an expression is not invertible and depends on the channel instantiation and the related unknown parameters. This calls for approximations leading to a tractable observation function.

C. Tractable Observation Function

We propose a tractable observation model obtained by considering:

- (i) the single-bounce model as in (4), i.e., $\boldsymbol{\alpha}^{(i)} \simeq \check{\boldsymbol{\alpha}}^{(i)} = [\check{\alpha}_1^{(i)}, \check{\alpha}_2^{(i)}, \ldots, \check{\alpha}_{m^{(i)}}^{(i)}]$;
- (ii) the amplitude of multipath components as constant within each time bin, i.e., $\overline{\alpha}_k^{(i)} \simeq \mathbb{E}_{\mathbf{p}_j \in \mathcal{E}_i}\left\{\check{\alpha}_j^{(i)} | \mathbf{p}_j\right\}$ for $\mathbf{p}_k \in \mathcal{E}_i$;
- (iii) the transmitted signal as an impulsive signal with respect to the time bin, i.e., $s(t_h)s(t_{h-k}) \simeq 0 \; \forall k \neq 0$ and $s(t - \tau_k) \simeq 0$ with $\tau_k \in \mathcal{T}_i \; \forall t \notin \mathcal{T}_i$.

Note that the accuracy of (i) and (ii) depends on T_d and on the signal bandwidth. In fact, the smaller T_d, the less the amplitude changes within a time interval and the more accurate the approximation (i) is. The larger is the bandwidth, the shorter is the signal's duration, especially with respect to the time interval, the more accurate is the approximation (ii). Therefore, such approximations are suitable for wideband ranging systems [26]. From (i) and (ii), the (23) becomes

$$\begin{aligned}\lambda_k^{(i)} &\simeq \frac{1}{\sigma_\text{n}^2} \overline{\alpha}_k \sum_{n \in \mathsf{N}_k^{(i)}} s^2(t_j - \check{\tau}_n^{(i)}) \\ &= |\mathsf{N}_k^{(i)}| \overline{\alpha}_k^2 \mathrm{S}_0\end{aligned} \tag{26}$$

where S_0 is the transmitted signal energy. In fact, based on the tractable observation model, the non-centrality parameter of the kth energy sample depends only on the targets located inside $\mathcal{E}_k^{(i)}$. Finally, we define the observation model as

$$\mathsf{n}_\text{t} = g(\mathbf{f}) + \mathsf{w} = \frac{1}{\overline{\alpha}_k^2 \mathrm{S}_0 n_\text{p}} \sum_{i=1}^{n_\text{p}} \sum_{k=1}^{n_\text{b}} \left(\frac{\mathsf{e}_k^{(i)}}{\sigma_\text{n}^2} - n_\text{sb} \right) + \mathsf{w} \tag{27}$$

where w is the measurement noise due to the difference between $\mathsf{f}_k^{(i)}$ and its expected value $\mathbb{E}\left\{\mathsf{f}_k^{(i)}\right\} = \lambda_k^{(i)}$.[15]

Remark 2: The crowd-counting solution based on energy detection leads to an intractable model for $\mathsf{n}_\text{t} = g(\boldsymbol{f})$ that is not invertible. Therefore, a tractable model is derived through approximations that are found to be accurate for wideband signals. In particular, the accuracy of the tractable model depends on the dwell time and the observation window of the energy detector. Such tractable model leads to (27), which is a linear function of the extracted features.

VI. Case Study

We now present the performance metrics, operating environment, signal processing, and numerical results for a case of study. The proposed crowd-centric method is compared with two other existing algorithms.

[15]The expected value is taken with respect to the additive white Gaussian noise (AWGN) noise.

A. Performance Metrics

As performance metrics, we consider the counting error, its root-mean-square (RMS), and the counting error outage (CEO). For an estimate $\hat{\mathsf{n}}_\mathsf{t}$ of n_t, the counting error in absolute value is $|\hat{\mathsf{n}}_\mathsf{t} - \mathsf{n}_\mathsf{t}|$. The counting RMSE is

$$e_{\text{rms}} = \sqrt{\mathbb{E}\left\{|\hat{\mathsf{n}}_\mathsf{t} - \mathsf{n}_\mathsf{t}|^2\right\}}. \tag{28}$$

The CEO is the probability that the counting error is above a certain value $n^\star$, and is defined as[16]

$$P_{\text{ceo}}(n^\star) = \mathbb{P}\{|\hat{\mathsf{n}}_\mathsf{t} - \mathsf{n}_\mathsf{t}| > n^\star\}. \tag{29}$$

B. Operating Environment

Consider a system composed of a transmitter at $\boldsymbol{p}_\text{T} = (3\,\text{m}, 5\,\text{m})$ and a receiver in $\boldsymbol{p}_\text{R} = (7\,\text{m}, 5\,\text{m})$. The transmitter emits pulses with rectangular frequency spectrum with lower frequency $f_\text{L} = 3.1\,\text{GHz}$ and upper frequency $f_\text{U} = 4.8\,\text{GHz}$, which is in agreement with the European lower band for UWB signals. The number of target scatterers n_t varies from 0 to $n_{\max} = 30$ and they are randomly located in a squared environment with origin in $\{(0\,\text{m}, 0\,\text{m})\}$ and side length of 10 m. The effect of spatial density is studied by varying the parameter ρ, i.e., the number of targets per squared meter in the environment.

The multipath amplitude from the different scatterers is modelled according to the IEEE 802.15.4 a standard for UWB systems, in particular by considering the indoor channel model. The signal-to-noise ratio (SNR) at 1 m from the transmitter is $\gamma_0 = 25\,\text{dB}$ unless otherwise stated.

C. Signal Processing

As for the individual-centric method, the ML estimation is considered as in (10) with $f(\tilde{\mathbf{r}}, \mathbf{p}_\mathsf{t}) = \tilde{f}(\tilde{\mathbf{r}}, \mathbf{p}_\mathsf{t})$ as in (17). Note that the performance obtained with ML estimation is used as a benchmark only, as its complexity has been found to be 400 times greater than the crowd-centric method for $n_{\max} = 10$, growing exponentially with $n_{\max}$, as described in Sec. II.

As for the crowd-centric method, four algorithms are considered, namely: (1) energy detector (ED); (2) window-threshold (WT); (3) active samples (AE); and (4) active duration (AD). The algorithms ED and WT do not require any learning phase and therefore are compared with the ML. The algorithm ED is the energy-based algorithm proposed in this paper. In particular, the energy detector at the receiver is set with an observation window of duration $T_{\text{obs}} = 100\,\text{ns}$. The estimation $\hat{\mathsf{n}}_\mathsf{t}$ is obtained from (27) as $\hat{\mathsf{n}}_\mathsf{t} = g(\mathbf{f})$. The average amplitude for the ith bin $\overline{\boldsymbol{\alpha}}_i$ is chosen by considering the approximation (ii) in Sec. (V-C). The duration of each bin is $T_\text{d} = 4\,\text{ns}$ unless otherwise stated.

The algorithm WT [17] is based on the power profile of the received signal $\tilde{\mathsf{r}}^{(i)}(t)$. Iteratively, a maximum search is performed on the power profile. If the maximum value overcomes a threshold, a target is detected and a set of samples (window) around the maximum is deleted. The maximum number of iterations is $n_{\max}$. In this paper, we consider the best case scenario (genie-aided) for this algorithm from the literature, where the threshold that minimizes the root-mean-square error (RMSE) is considered. Unless otherwise stated, the window length is set equal to the duration of a transmitted pulse. However, results are shown for different values of window length.

[16]This performance metric is close to the bit error outage used for communication systems [57]–[59].

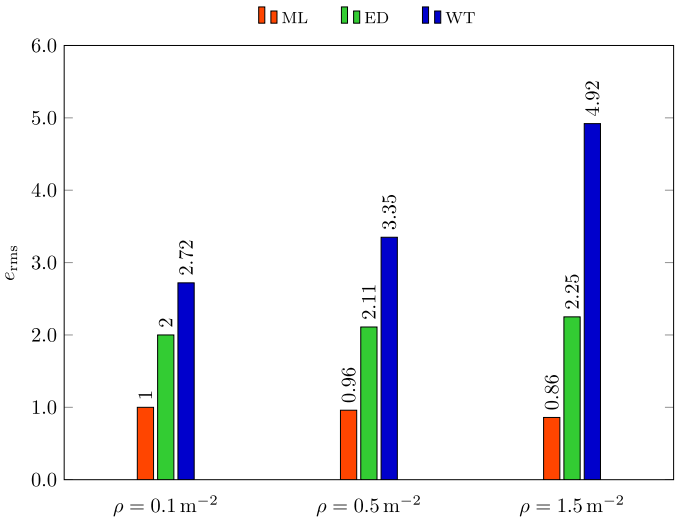

Fig. 5. Counting RMSE error for $n_{\max} = 10$ for $\gamma_0 = 20\,\text{dB}$. The results obtained with ML, ED, and WT are compared for different values of target spatial density ρ.

D. Numerical Results

Fig. 5 shows the counting RMSE e_{rms} for three different values of spatial density $\rho = 0.1, 0.5,$ and $1.5\,\text{m}^{-2}$, $n_{\max} = 10$, and $\gamma_0 = 20\,\text{dB}$ for the ML, ED, and WT algorithms. It can be observed that the RMSE for the ML algorithm does not increase with the spatial density, for example $e_{\text{rms}} = 1$ for $\rho = 0.1\,\text{m}^{-2}$ and $e_{\text{rms}} = 0.86$ for $\rho = 1.5\,\text{m}^{-2}$. Differently, the RMSE for the proposed ED algorithm is $e_{\text{rms}} = 2$ for $\rho = 0.1\,\text{m}^{-2}$ and $e_{\text{rms}} = 2.25$ for $\rho = 1.5\,\text{m}^{-2}$. However, the WT algorithm is the most sensitive to the spatial density, with $e_{\text{rms}} = 2.72$ for $\rho = 0.1\,\text{m}^{-2}$ and $e_{\text{rms}} = 4.92$ for $\rho = 1.5\,\text{m}^{-2}$. This can be attributed to the fact that when ρ increases it is more likely to have overlapping signal replicas due to targets that are closer in space. If an energy bin includes the energy of different signal replicas, the corresponding non-centrality parameter (and therefore $\mathbf{f}$) has higher variance, resulting in

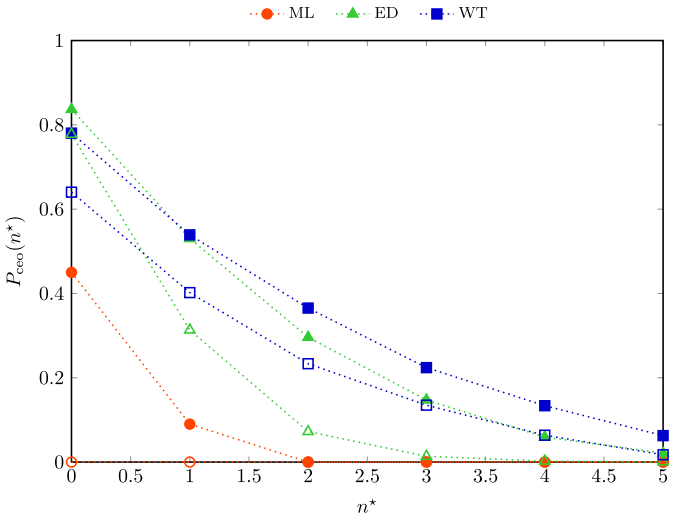

Fig. 6. CEO for $n_{\max} = 10$ as a function of $n^\star$. The results obtained with ML, ED, and WT are compared for $\gamma_0 = 20\,\text{dB}$ (full markers) and $\gamma_0 = 25\,\text{dB}$ (empty markers).

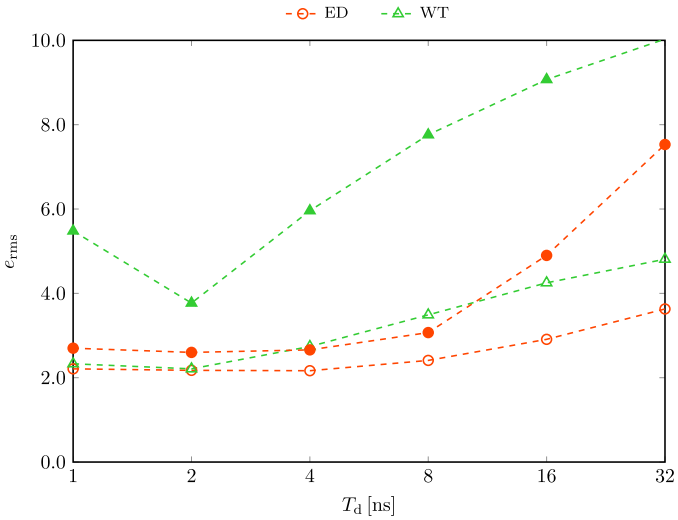

Fig. 7. Counting RMSE vs. T_{d} obtained with ED and WT, where both the ED dwell time and the WT window length are set to T_{d}, $n_{\max} = 10$, $\gamma_0 = 20\,\text{dB}$ (full markers) and $\gamma_0 = 25\,\text{dB}$ (empty markers).

the increased error for the proposed ED algorithm. As for the WT algorithm, if the local maximum at one iteration is above the threshold, a single target is detected even if the maximum value is due to different targets leading to overlapping signal replicas. Therefore, the WT is more sensitive to the spatial density as it considers only the arrival time disregarding the signal amplitude.

Fig. 6 shows the CEO as a function of $n^\star$ for the ML, ED, and WT algorithms with $\gamma_0 = 20\,\text{dB}$ and $25\,\text{dB}$. It can be observed that the proposed ED algorithm outperforms the WT algorithm for both the values of γ_0. Also, the ED algorithm is more sensitive to the SNR. In particular, the counting error obtained with the ED algorithm is below $n^\star = 2$ in the 70% of cases for $\gamma_0 = 20\,\text{dB}$ and 93% of cases for $\gamma_0 = 25\,\text{dB}$, which is close to the benchmark represented by the ML case. The counting error obtained with the WT algorithm is below $n^\star = 2$ in the 64% of cases for $\gamma_0 = 20\,\text{dB}$ and 77% of cases for $\gamma_0 = 25\,\text{dB}$. This can be attributed to the fact that when γ_0 increases the variance of the energy bins decreases and therefore the energy-based estimation is more accurate. Differently, as the WT algorithm considers only the arrival time, this effect is less important.

Fig. 7 shows the counting RMSE for the ED and WT algorithms as a function of T_{d}, when both the dwell time for the ED algorithm and the window length for the WT algorithm are set to T_{d} for $\gamma_0 = 20\,\text{dB}$ (full markers) and $\gamma_0 = 25\,\text{dB}$ (empty markers). It can be observed that the WT is more sensitive to the window length. For $\gamma_0 = 20$, the counting RMSE is $e_{\text{rms}} = 4$ for $T_{\text{d}} = 2\,\text{ns}$ and $e_{\text{rms}} = 10$ for $T_{\text{d}} = 32\,\text{ns}$. The RMSE for the proposed ED algorithm is 3.6 when $\gamma_0 = 25\,\text{dB}$ and 7.5 when $\gamma_0 = 20$. In fact, higher values of the variance of the energy bins, and therefore that of $\mathbf{f}$, corresponds to lower values of SNR. This result highlights that the window length is a crucial parameter for the performance of the WT. Also, the proposed ED algorithm is less sensitive to the value of the dwell time.

Fig. 8 shows an example of the estimate $\hat{\mathsf{n}}_{\mathsf{t}}$ for the proposed ED, together with WT, AE, and AD algorithms, as a function of the true value n_{t} that varies from 1 to 30. It can be noticed that the proposed ED algorithm outperforms all the other algorithms in terms of both mean value and confidence interval. The 95% confidence interval of the counting error for $\mathsf{n}_{\mathsf{t}} = 15$ is $(12.0, 18.4)$ with mean value 15.2 for the ED algorithm, $(5.3, 11.5)$ with mean value 8.5 for the TW algorithm; $(9.5, 21.9)$ with mean value 15.7 for the ED algorithm; $(9.4, 22.2)$ with mean value 15.8 for the ED algorithm. As expected, the WT algorithm has a greater error for higher values of n_{t} as the target spatial density increases with n_{t}. The regression-based algorithms AE and AD show good performance in terms of expected value but their standard deviation is higher than that of the ED algorithm.

Fig. 9 shows the correlation between the feature $\mathbf{f}$ and the true number of targets as a function of the threshold-to-noise ratio (TNR), which is the ratio between the threshold used in the algorithms and the noise power. Such correlation is based on the Pearson's correlation coefficient, which indicates whether a monotone relation between the two variables exists [60]. It can be noticed that the maximum correlation is obtained with the proposed ED algorithm and is 0.98, which is constant because the ED does not involve a threshold comparison, whereas it is 0.93 for the AE, 0.94 for the AD, and 0.92 for the TW. This results confirm the importance of the threshold design.

Fig. 10 shows the CEO as a function of $n^\star$ for the proposed ED, together with WT, AE, and AD algorithms, with $n_{\max} = 30$. It can be observed that the proposed ED algorithm outperforms all the other algorithms, whereas the worst performance are obtained with the WT algorithm. In particular, the counting error is below 2 in the 88% of cases for the ED, 65% of cases for the AE, 68% of cases for the

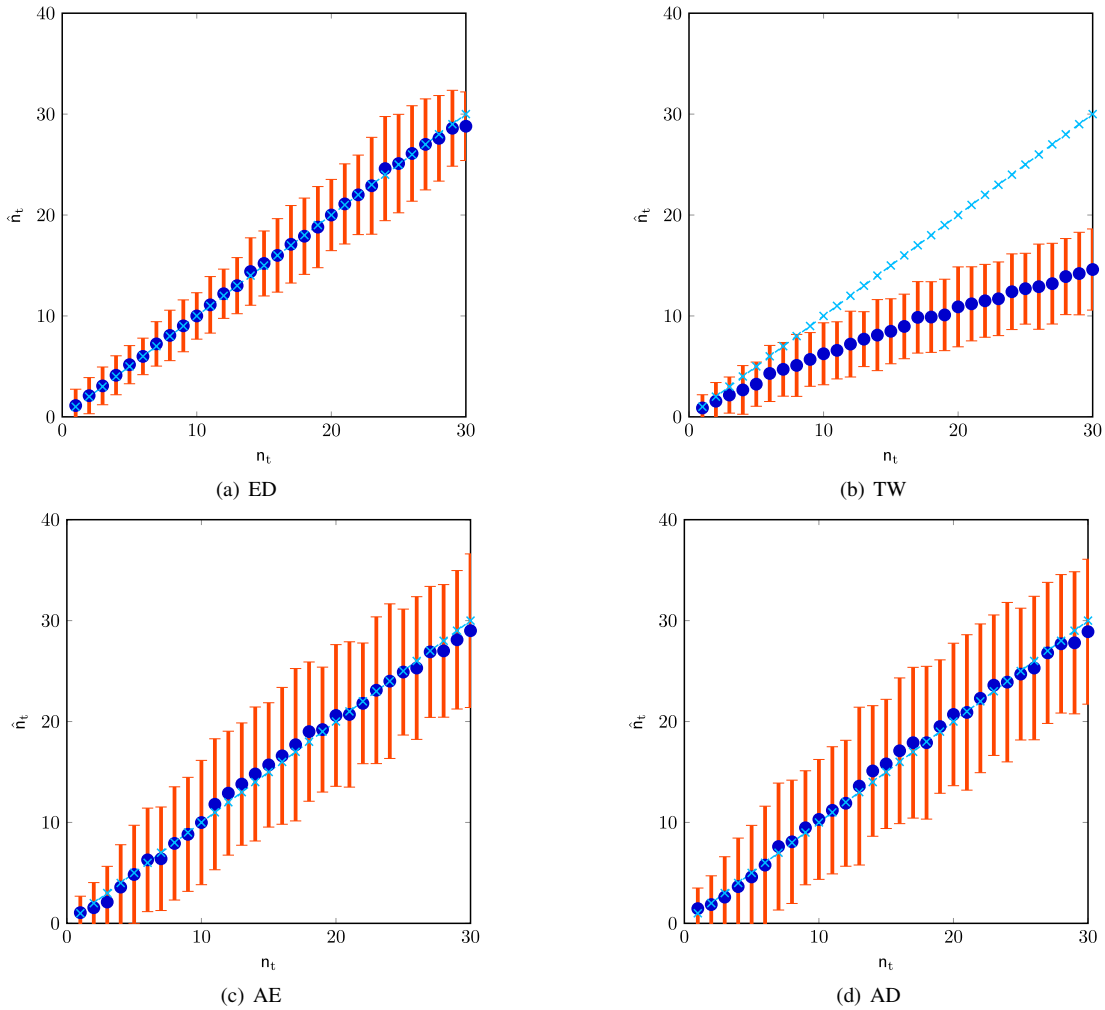

Fig. 8. Example of estimated number of targets $\hat{n}_t$ as a function of the true number of targets n_t for the four algorithms ED, TW, AE, and AD. The red error bars indicate the 95% confidence interval calculated over 100 random positions, the blue dot indicates the average value, and the cyan crosses indicates the bisector (i.e., the ideal case $\hat{n}_t = n_t$).

AD, and 33% of cases for the TW. This result confirms the superior performance of our proposed method compared to the existing crowd-centric algorithms.

VII. Conclusion

This paper presents a device-free counting system based on sensor radars. Two different methods have been proposed: the individual-centric, based on model order selection, and the crowd-centric, based on energy-detection. A tractable model for energy detection is developed for counting. Such a model led to a simple expression for the value of energy samples as a function of the number of targets. This function is particularly accurate when wideband and ultra-wideband signals are employed. The individual-centric approach outperforms the crowd-centric one in terms of performance, but leads to a computational complexity that increases exponentially with the maximum number of targets and to a running time of two orders of magnitude greater than that of the crowd-centric even for only ten targets. The crowd-centric approach has a complexity that does not depend on the number of targets and thus opens the way to a variety of device-free applications.

Acknowledgments

The authors wish to thank Z. Liu and N. Tadayon for the careful reading of the manuscript.

References

[1] E. Cianca, M. D. Sanctis, and S. D. Domenico, "Radios as sensors," *IEEE Internet of Things Journal*, 2016, to appear.
[2] S. Savazzi, S. Sigg, M. Nicoli, V. Rampa, S. Kianoush, and U. Spagnolini, "Device-free radio vision for assisted living: Leveraging wireless channel quality information for human sensing," *IEEE Signal Process. Mag.*, vol. 33, no. 2, pp. 45–58, Mar. 2016.
[3] Y. L. Hou and G. K. H. Pang, "People counting and human detection in a challenging situation," *IEEE Transactions on Systems, Man, and Cybernetics - Part A: Systems and Humans*, vol. 41, no. 1, pp. 24–33, Jan 2011.
[4] N. C. Tang, Y. Y. Lin, M. F. Weng, and H. Y. M. Liao, "Cross-camera knowledge transfer for multiview people counting," *IEEE Transactions on Image Processing*, vol. 24, no. 1, pp. 80–93, Jan 2015.
[5] B. K. Dan, Y. S. Kim, Suryanto, J. Y. Jung, and S. J. Ko, "Robust people counting system based on sensor fusion," *IEEE Transactions on Consumer Electronics*, vol. 58, no. 3, pp. 1013–1021, August 2012.
[6] A. B. Chan and N. Vasconcelos, "Counting people with low-level features and Bayesian regression," *IEEE Transactions on Image Processing*, vol. 21, no. 4, pp. 2160–2177, April 2012.
[7] A. Basalamah, "Sensing the crowds using bluetooth low energy tags," *IEEE Access*, vol. 4, pp. 4225–4233, Aug. 2016.

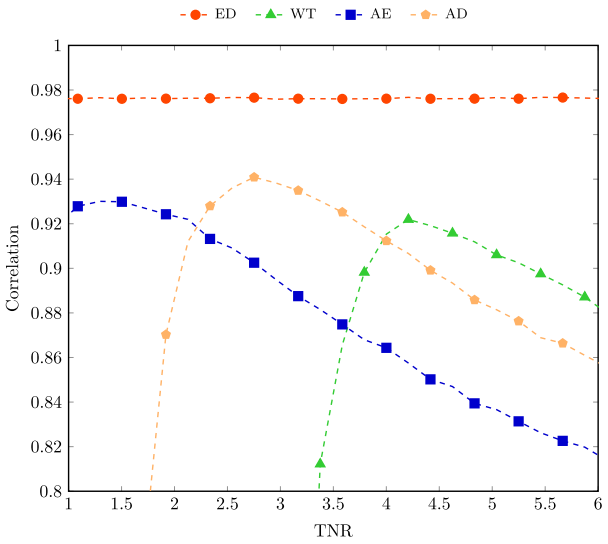

Fig. 9. Pearson's correlation coefficient between $\mathbf{f}$ and n_{t} for the ML, TW, AE, AD as a function of the threshold-to-noise ratio.

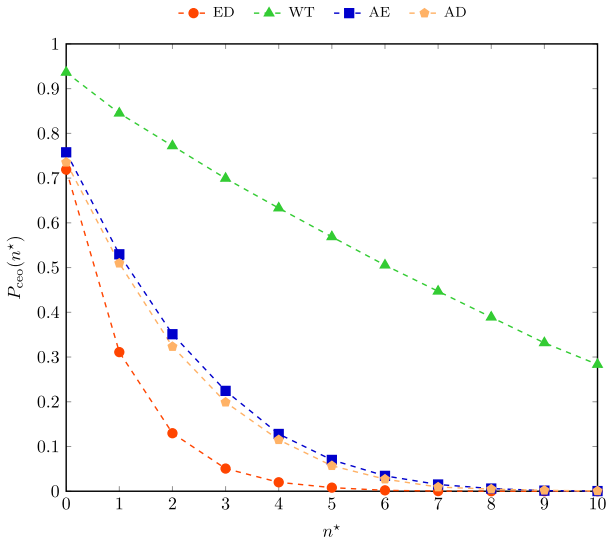

Fig. 10. CEO as a function of $n^{\star}$ for the ED, WT, AE, and AS algorithms and $n_{\max} = 30$.

[8] H. Han, B. Sheng, C. C. Tan, Q. Li, W. Mao, and S. Lu, "Counting rfid tags efficiently and anonymously," in *INFOCOM, 2010 Proceedings IEEE*, San Diego, CA, USA, Mar. 2010, pp. 1–9.

[9] F. Guidi, N. Decarli, S. Bartoletti, A. Conti, and D. Dardari, "Detection of multiple tags based on impulsive backscattered signals," *IEEE Trans. Commun.*, vol. 62, no. 11, pp. 3918–3930, Nov. 2014.

[10] H. Li, E. C. L. Chan, X. Guo, J. Xiao, K. Wu, and L. M. Ni, "Wi-counter: Smartphone-based people counter using crowdsourced Wi-Fi signal data," *IEEE Transactions on Human-Machine Systems*, vol. 45, no. 4, pp. 442–452, Aug 2015.

[11] W. Xi, J. Zhao, X. Y. Li, K. Zhao, S. Tang, X. Liu, and Z. Jiang, "Electronic frog eye: Counting crowd using WiFi," in *IEEE INFOCOM 2014 - IEEE Conference on Computer Communications*, April 2014, pp. 361–369.

[12] S. Depatla, A. Muralidharan, and Y. Mostofi, "Occupancy estimation using only WiFi power measurements," *IEEE Journal on Selected Areas in Communications*, vol. 33, no. 7, pp. 1381–1393, July 2015.

[13] E. Vattapparamban, B. S. Ciftler, I. Guvenc, K. Akkaya, and A. Kadri, "Indoor occupancy tracking in smart buildings using passive sniffing of probe requests," in *2016 IEEE International Conference on Communications Workshops (ICC)*, May 2016, pp. 38–44.

[14] K. K. Mada, H.-C. Wu, and S. S. Iyengar, "Efficient and robust EM algorithm for multiple wideband source localization," *IEEE Trans. Veh. Technol.*, vol. 58, no. 6, pp. 3071–3075, Jul. 2009.

[15] L. Lu, H. Zhang, and H.-C. Wu, "Novel energy-based localization technique for multiple sources," *IEEE Syst. J.*, vol. 8, no. 1, pp. 142–150, Mar. 2014.

[16] X. Quan, J. W. Choi, and S. H. Cho, "In-bound/out-bound detection of people's movements using an IR-UWB radar system," in *Int. Conf. on Electronics, Information and Communications (ICEIC)*, Kota Kinabalu, Malaysia, Jan. 2014, pp. 1–2.

[17] J. W. Choi, J. H. Kim, and S. H. Cho, "A counting algorithm for multiple objects using an IR-UWB radar system," in *IEEE Int. Conf. on Net. Infrastr. and Digital Content*, Beijing, China, Sep. 2012, pp. 591–595.

[18] J. He and A. Arora, "A regression-based radar-mote system for people counting," in *Pervasive Computing and Communications (PerCom), 2014 IEEE International Conference on*, Louis Missouri, USA, Mar. 2014, p. 95102.

[19] R. Niu and P. K. Varshney, "Target location estimation in sensor networks with quantized data," *IEEE Trans. Signal Process.*, vol. 54, no. 12, pp. 4519–4528, Dec. 2006.

[20] R. Niu, R. S. Blum, P. K. Varshney, and A. L. Drozd, "Target localization and tracking in noncoherent multiple-input multiple-output radar systems," *IEEE Trans. Aerosp. Electron. Syst.*, vol. 48, no. 2, pp. 1466–1489, Apr. 2012.

[21] M. I. Skolnik, *Radar Handbook*, 2nd ed. McGraw-Hill Professional, Jan. 1990.

[22] V. S. Chernyak, *Fundamentals of Multisite Radar Systems: Multistatic Radars and Multistatic Radar Systems*. London, U.K.: CRC Press, 1998.

[23] M. Z. Win and R. A. Scholtz, "Impulse radio: How it works," *IEEE Commun. Lett.*, vol. 2, no. 2, pp. 36–38, Feb. 1998.

[24] ——, "Ultra-wide bandwidth time-hopping spread-spectrum impulse radio for wireless multiple-access communications," *IEEE Trans. Commun.*, vol. 48, no. 4, pp. 679–691, Apr. 2000.

[25] L. Yang and G. B. Giannakis, "Ultra-wideband communications: An idea whose time has come," *IEEE Signal Process. Mag.*, vol. 21, no. 6, pp. 26–54, Nov. 2004.

[26] S. Bartoletti, W. Dai, A. Conti, and M. Z. Win, "A mathematical model for wideband ranging," *IEEE J. Sel. Topics Signal Process.*, vol. 9, no. 2, pp. 216–228, Mar. 2015.

[27] S. Bartoletti, A. Giorgetti, M. Z. Win, and A. Conti, "Blind selection of representative observations for sensor radar networks," *IEEE Trans. Veh. Technol.*, vol. 64, no. 4, pp. 1388–1400, Apr. 2015.

[28] S. Gezici and H. V. Poor, "Position estimation via ultra-wide-band signals," *Proc. IEEE*, vol. 97, no. 2, pp. 386–403, Feb. 2009.

[29] S. Gezici, Z. Tian, G. B. Giannakis, H. Kobayashi, A. F. Molisch, H. V. Poor, and Z. Sahinoglu, "Localization via ultra-wideband radios: A look at positioning aspects for future sensor networks," *IEEE Signal Process. Mag.*, vol. 22, no. 4, pp. 70–84, Jul. 2005.

[30] Y. Shen, S. Mazuelas, and M. Z. Win, "Network navigation: Theory and interpretation," *IEEE J. Sel. Areas Commun.*, vol. 30, no. 9, pp. 1823–1834, Oct. 2012. [Online]. Available: http://arxiv.org/abs/1112.3599

[31] Y. Shen and M. Z. Win, "Fundamental limits of wideband localization – Part I: A general framework," *IEEE Trans. Inf. Theory*, vol. 56, no. 10, pp. 4956–4980, Oct. 2010. [Online]. Available: http://arxiv.org/abs/1006.0888v1

[32] ——, "On the accuracy of localization systems using wideband antenna arrays," *IEEE Trans. Commun.*, vol. 58, no. 1, pp. 270–280, Jan. 2010.

[33] R. J. Fontana and S. J. Gunderson, "Ultra-wideband precision asset location system," *Proc. IEEE Conf. on Ultra Wideband Syst. and Technol.*, vol. 21, no. 1, pp. 147–150, May 2002.

[34] D. Dardari, A. Conti, U. J. Ferner, A. Giorgetti, and M. Z. Win, "Ranging with ultrawide bandwidth signals in multipath environments," *Proc. IEEE*, vol. 97, no. 2, pp. 404–426, Feb. 2009, special issue on *Ultra-Wide Bandwidth (UWB) Technology & Emerging Applications*.

[35] A. A. Saleh and R. A. Valenzuela, "A statistical model for indoor multipath propagation," *IEEE J. Sel. Areas Commun.*, vol. 5, no. 2, pp. 128–137, Feb. 1987.

[36] A. Meijerink and A. F. Molisch, "On the physical interpretation of the saleh-valenzuela model and the definition of its power delay profiles," *IEEE Trans. Antennas Propag.*, vol. 62, no. 9, pp. 4780–4793, Sep. 2014.

[37] A. F. Molisch, "Ultra-wideband communications: An overview," *Radio Science Bulletin*, no. 329, pp. 31–42, Jun. 2009.

[38] ——, *Wireless Communications*, 2nd ed. United Kingdom: IEEE Press, John Wiley & Sons Ltd., 2010.

[39] A. F. Molisch, D. Cassioli, C.-C. Chong, S. Emami, A. Fort, B. Kannan, J. Karedal, J. Kunisch, H. Schantz, K. Siwiak, and M. Z. Win, "A comprehensive standardized model for ultrawideband propagation channels," *IEEE Trans. Antennas Propag.*, vol. 54, no. 11, pp. 3151–3166, Nov. 2006, special issue on *Wireless Communications*.
[40] S. Bartoletti, A. Conti, and A. Giorgetti, "Analysis of UWB radar sensor networks," in *Proc. IEEE Int. Conf. Commun.*, Cape Town, South Africa, May 2010, pp. 1–6.
[41] P. Stoica and Y. Selen, "Model-order selection: a review of information criterion rules," *IEEE Signal Process. Mag.*, vol. 21, no. 4, pp. 36–47, 2004.
[42] J. Aspnes, D. Goldenberg, and Y. R. Yang, "On the computational complexity of sensor network localization," in *Proc. of First Int. Workshop on Algorithmic Aspects of Wireless Sensor Networks*. Springer-Verlag, 2004, pp. 32–44.
[43] H. Urkowitz, "Energy detection for unknown deterministic signal," *Proc. IEEE*, vol. 55, no. 4, pp. 523–531, Apr. 1967.
[44] C. Xu and C. L. Law, "Delay-dependent threshold selection for UWB TOA estimation," *IEEE Commun. Lett.*, vol. 12, no. 5, pp. 380–382, May 2008.
[45] A. Giorgetti and M. Chiani, "Time-of-arrival estimation based on information theoretic criteria," *IEEE Trans. Signal Process.*, vol. 61, no. 8, pp. 1869–1879, Apr. 2013.
[46] X. Cheng, F. Vanhaverbeke, Y. L. Guan, and M. Moeneclaey, "Blind combining for weighted energy detection of UWB signals," *Electron. Lett.*, vol. 47, no. 1, pp. 55–57, Jan. 2011.
[47] S. Xie, Y. Liu, Y. Zhang, and R. Yu, "A parallel cooperative spectrum sensing in cognitive radio networks," *IEEE Trans. Veh. Technol.*, vol. 59, no. 8, pp. 4079–4092, Oct. 2010.
[48] A. Mariani, A. Giorgetti, and M. Chiani, "Effects of noise power estimation on energy detection for cognitive radio applications," *IEEE Trans. Commun.*, vol. 59, no. 12, pp. 3410–3420, Dec. 2011.
[49] E. Axell, G. Leus, E. G. Larsson, and H. V. Poor, "Spectrum sensing for cognitive radio: state-of-the-art and recent advances," *IEEE Signal Process. Mag.*, vol. 29, no. 3, pp. 101–116, May 2012.
[50] J. W. Chong, D. K. Sung, and Y. Sung, "Cross-layer performance analysis for CSMA/CA protocols: Impact of imperfect sensing," *IEEE Trans. Veh. Technol.*, vol. 59, no. 3, pp. 1100–1108, Mar. 2010.
[51] L. Ye, Z. Zhang, J. Zhang, and H. Zhang, "Carrier sensing with self-cancelation of inter-carrier emission in cognitive OFDMA system," in *Proc. IEEE Int. Conf. Commun.*, Kyoto, Japan, Jun. 2011, pp. 1–6.
[52] I. Ramachandran and S. Roy, "Clear channel assessment in energy-constrained wideband wireless networks," *IEEE Wireless Commun. Mag.*, vol. 14, no. 3, pp. 70–78, Jun. 2007.
[53] A. Rabbachin, T. Q. Quek, P. C. Pinto, I. Oppermann, and M. Z. Win, "Non-coherent UWB communication in the presence of multiple narrowband interferers," *IEEE Trans. Wireless Commun.*, vol. 9, no. 11, pp. 3365–3379, Nov. 2010.
[54] A. Rabbachin, I. Oppermann, and B. Denis, "GML ToA estimation based on low complexity UWB energy detection," in *Proc. IEEE Int. Symp. on Personal, Indoor and Mobile Radio Commun.*, Helsinki, Finland, Sep. 2006, pp. 1–5.
[55] ——, "ML Time-of-Arrival estimation based on low complexity UWB energy detection," in *Proc. IEEE Int. Conf. on Ultra-Wideband*, Waltham, MA, Sep. 2006, pp. 599–604.
[56] L. Stoica, A. Rabbachin, and I. Oppermann, "A low-complexity non-coherent IR-UWB transceiver architecture with TOA estimation," *IEEE Trans. Microw. Theory Tech.*, vol. 54, no. 4, pp. 1637–1646, Jun. 2006.
[57] A. Conti, M. Z. Win, M. Chiani, and J. H. Winters, "Bit error outage for diversity reception in shadowing environment," *IEEE Commun. Lett.*, vol. 7, no. 1, pp. 15–17, Jan. 2003.
[58] A. Conti, M. Z. Win, and M. Chiani, "Invertible bounds for M-QAM in fading channels," *IEEE Trans. Wireless Commun.*, vol. 4, no. 5, pp. 1994–2000, Sep. 2005.
[59] A. Conti, W. M. Gifford, M. Z. Win, and M. Chiani, "Optimized simple bounds for diversity systems," *IEEE Trans. Commun.*, vol. 57, no. 9, pp. 2674–2685, Sep. 2009.
[60] N. Balakrishnan and C. D. Lai, *Continuous Bivariate Distributions*, 2nd ed. Springer, 2009.

Stefania Bartoletti (S'12) received the Laurea degree (*summa cum laude*) in electronics and telecommunications engineering and the Ph.D. degree in information engineering from the University of Ferrara, Italy, in 2011 and 2015, respectively.

Since June 2016, she is recipient of a Marie Skłodowska-Curie Global Fellowship within the H2020 European Framework for a research project with the Massachusetts Institute of Technology and the University of Ferrara. Her research interests include theory and experimentation of wireless networks for passive localization and physical behavior analysis. She is recipient of the 2016 Paul Baran Young Scholar Award of the Marconi Society.

Dr. Bartoletti served as a Chair of the TPC for the 2017 IEEE ICC Workshop on Advances in Network Localization and Navigation (ANLN), and as reviewer for numerous IEEE journals and international conferences.

Andrea Conti (S'99-M'01-SM'11) received the Laurea (*summa cum laude*) in telecommunications engineering and the Ph.D. in electronic engineering and computer science from the University of Bologna, Italy, in 1997 and 2001, respectively.

He is an Associate Professor at the University of Ferrara, Italy. His research interests involve theory and experimentation of wireless systems and networks including network localization, adaptive diversity communications, network secrecy, and multidimensional random sampling. He is recipient of the HTE Puskás Tivadar Medal and co-recipient of the IEEE Communications Society's Stephen O. Rice Prize and the IEEE Communications Society's Fred W. Ellersick Prize.

Dr. Conti has served as editor for IEEE journals, as well as organized and chaired numerous international conferences over the last decade. He was elected Chair of the IEEE Communications Society's Radio Communications Technical Committee. He is an elected Fellow of the IET and has been selected as an IEEE Distinguished Lecturer.

Moe Z. Win (S'85-M'87-SM'97-F'04) received both the Ph.D. in Electrical Engineering and the M.S. in Applied Mathematics as a Presidential Fellow at the University of Southern California (USC) in 1998. He received the M.S. in Electrical Engineering from USC in 1989 and the B.S. (*magna cum laude*) in Electrical Engineering from Texas A&M University in 1987.

He is a Professor at the Massachusetts Institute of Technology (MIT) and the founding director of the Wireless Information and Network Sciences Laboratory. Prior to joining MIT, he was with AT&T Research Laboratories for five years and with the Jet Propulsion Laboratory for seven years. His research encompasses fundamental theories, algorithm design, and experimentation for a broad range of real-world problems. His current research topics include network localization and navigation, network interference exploitation, intrinsic wireless secrecy, adaptive diversity techniques, and ultra-wideband systems.

Dr. Win is an elected Fellow of the AAAS, the IEEE, and the IET, and was an IEEE Distinguished Lecturer. He was honored with two IEEE Technical Field Awards: the IEEE Kiyo Tomiyasu Award (2011) and the IEEE Eric E. Sumner Award (2006, jointly with R. A. Scholtz). Together with students and colleagues, his papers have received numerous awards. Other recognitions include the IEEE Communications Society Edwin H. Armstrong Achievement Award (2016), the International Prize for Communications Cristoforo Colombo (2013), the *Laurea Honoris Causa* from the University of Ferrara (2008), the Technical Recognition Award of the IEEE ComSoc Radio Communications Committee (2008), and the U.S. Presidential Early Career Award for Scientists and Engineers (2004).

Dr. Win was an elected Member-at-Large on the IEEE Communications Society Board of Governors (2011–2013). He was the Chair (2005–2006) and Secretary (2003–2004) for the Radio Communications Committee of the IEEE Communications Society. Over the last decade, he has served as editor for IEEE journals, as well as organized and chaired numerous international conferences. He is currently serving on the SIAM Diversity Advisory Committee.